

[¹⁸F]SF5I, a novel ¹⁸F-labeled PET radioligand for translocator protein 18kDa (TSPO) in brain, works well in monkeys but fails in humans

Journal of Cerebral Blood Flow & Metabolism
0(0) 1–8
© The Author(s) 2024
Article reuse guidelines:
sagepub.com/journals-permissions
DOI: 10.1177/0271678X241304924
journals.sagepub.com/home/jcbfm



Xuefeng Yan, Fabrice G Siméon, Jeih-San Liow, Cheryl L Morse, Susovan Jana , Jose A Montero Santamaria, Madeline Jenkins, Sami S Zoghbi, Victor W Pike, Robert B Innis and Paolo Zanotti-Fregonara

Abstract

[¹⁸F]SF5I is a novel radioligand for imaging translocator protein 18 kDa (TSPO) that previously displayed excellent imaging properties in nonhuman primates. This study assessed its performance in human brain and its dosimetry. Seven healthy participants underwent brain PET imaging to measure TSPO binding using a two-tissue compartment model (2TCM) to calculate total distribution volume (V_T). This cohort included two high-affinity binders (HABs), three mixed-affinity binders (MABs), and two low-affinity binders (LABs). Two other participants received whole-body scans to assess radiation exposure. Peak brain radioactivity reached a standardized uptake value (SUV) of 1.4 at 3 minutes post-injection, diminishing to 30% of peak by 120 minutes. The average V_T for all genotype groups was notably low ($<1 \text{ mL}\cdot\text{cm}^{-3}$), emphasizing the radioligand's poor binding in brain. [¹⁸F]SF5I remained sensitive to the TSPO polymorphism *in vivo*, as shown by a two-fold difference in V_T between HABs and LABs. V_T stabilization by 80 minutes post-injection suggested minimal radiometabolite accumulation in brain. The average effective dose was $13.8 \pm 0.9 \mu\text{Sv}/\text{MBq}$. Contrary to previously published animal data, [¹⁸F]SF5I showed low binding to human TSPO, with uptake remaining influenced by the rs6971 polymorphism. These findings highlight the challenges of developing TSPO radioligands and underscore the significant species differences that may influence translational outcomes.

ClinicalTrials.gov identifier: NCT05564429; registered 10/03/2022

Keywords

Brain scanning, human, PET imaging, TSPO, whole body scanning

Received 9 August 2024; Revised 24 October 2024; Accepted 8 November 2024

Introduction

Translocator protein 18 kDa (TSPO) is present in various cell types in brain, including glial cells (such as astrocytes and microglia) and endothelial cells, and is a widely recognized marker for neuroinflammation.^{1–3} Positron emission tomography (PET) imaging targeting TSPO has become instrumental in identifying and quantifying neuroinflammatory responses.^{4–7} Although TSPO expression in rodents is closely linked to microglial activation, recent human studies suggest that TSPO PET imaging may reflect general inflammation without specifying individual cell types.^{8,9} Although its function remains only partially elucidated,¹⁰ TSPO continues to hold significant potential for both

research and clinical management of neuroinflammatory diseases.¹¹

Our laboratory previously developed [¹¹C]ER176,¹² a radioligand with high specific binding and lack of radiometabolites entering the brain.¹³ In a comparison with other commonly used TSPO tracers, [¹¹C]ER176

Molecular Imaging Branch, National Institute of Mental Health, National Institutes of Health, Bethesda, MD, USA

Corresponding author:

Robert Innis, Molecular Imaging Branch, NIMH/NIH, 10 Center Drive, Bethesda, MD 20892, USA.
Email: robert.innis@nih.gov

had the most favorable imaging characteristics.¹⁴ In particular, the high specific binding of [¹¹C]ER176 allows the imaging of individuals with low-affinity binding,¹³ as determined by the *rs6971* TSPO polymorphism.¹⁵ Labeling with ¹¹C, however, precludes its use in centers without a cyclotron on site. In an effort to create an ¹⁸F-labeled analog of [¹¹C]ER176, our laboratory tested [¹⁸F]SF51 in nonhuman primates and found excellent imaging characteristics, including high specific to background uptake ($BP_{ND} = 7.6 \pm 4.3$) and robust quantification with a two-tissue compartment model (2TCM).¹⁶

The present study evaluated [¹⁸F]SF51's ability to quantify TSPO in healthy human brain. In particular, the study sought to assess whether [¹⁸F]SF51, which has a similar structure to [¹¹C]ER176, was capable of effectively imaging individuals with the three different TSPO affinity profiles. Towards this end, the brains of seven participants with high, mixed, and low affinity to TSPO were imaged. Two additional participants were enrolled to calculate radiation exposure.

Material and methods

Radiochemistry

Synthesis of [¹⁸F]SF51 was performed by a new radio-fluorination procedure that will be described elsewhere. The [¹⁸F]SF51 produced for this human study was analyzed with a battery of quality control procedures to explore the full range of parameters necessary to proceed with the study under a US Food and Drug Administration (FDA) Investigational New Drug (IND) indication (e.g., radiochemical purity, chemical purity, molar activity, stability, etc).

Participants

Nine healthy volunteers participated in the study and were genotyped for the *rs6971* TSPO polymorphism to designate them according to their TSPO affinities for second-generation radioligands. This cohort included two high-affinity binders (HABs), five mixed-affinity binders (MABs), and two low-affinity binders (LABs). Seven of the participants underwent brain PET scans; these included one male and one female with HAB status, one male and one female with LAB status, and two males and one female with MAB status (45 ± 9 years). Two additional participants with MAB status had whole-body PET scans to calculate dosimetry (one female, one male, 42 ± 8 years). All participants underwent comprehensive medical and psychiatric evaluations, including a medical history review, physical examination, electrocardiogram, and

blood tests. The study was approved by the National Institutes of Health (NIH) Combined Neurosciences Institutional Review Board (protocol number: 000674; ClinicalTrials.gov identifier: NCT05564429), in accordance with the Declaration of Helsinki. All participants provided written informed consent prior to enrollment in the study.

Brain scan procedures and processing

Each participant underwent a single PET scan, either brain ($n=7$) or whole body ($n=2$). The scans were performed with a Biograph mCT scanner (Siemens Medical Solution, Cary, NC, USA). To correct for attenuation, a preliminary low-dose CT scan was conducted, followed by intravenous administration of [¹⁸F]SF51. PET data were acquired over 120 minutes, with simultaneous arterial blood sampling. Each participant also underwent T1-weighted MR imaging on a 3T Philips Achieva (Bothell, WA, USA) for anatomical reference. The PET and MRI data were then processed using co-registration, segmentation, and atlas normalization techniques.¹⁷

Radioligand and radiometabolite analysis in plasma

Plasma concentrations of unchanged [¹⁸F]SF51 were measured at prescribed intervals from arterial blood samples using a previously defined standard method.¹⁸ Blood samples were collected at 15-second intervals during the first 3 minutes; at 5-minute intervals from 5 to 15 minutes; and at 15-minute intervals after 15 minutes, up to 120 minutes. The concentration of parent radioligand was measured in each plasma sample after separating it from whole blood as previously described.¹⁸ The free parent fraction in plasma (f_P) was measured in triplicate and normalized using an internal standard.¹⁹

Kinetic analysis

The total distribution volume (V_T) was calculated using 2TCM based on brain time-activity curves and radiometabolite-corrected arterial input function. Brain PET data were analyzed using PMOD software (PMOD Technologies Ltd., Zurich, Switzerland).

Whole-body biodistribution and radiation dosimetry

Radiation exposure was measured via whole-body PET scans using OLINDA/EXM version 1.1 software, as previously described.¹⁷

Statistical analysis

All statistical analyses were performed using GraphPad Prism (version 5.02, GraphPad Software, Inc.,

San Diego, California). Data from PET imaging and blood input measurements are presented as mean \pm standard deviation (SD). Differences in the fraction of unchanged [^{18}F]SF51 (f_p values) among HABs, MABs, and LABs were evaluated using one-way analysis of variance (ANOVA). A p-value of less than 0.05 was considered statistically significant.

Results

Injection parameters and pharmacological effects

[^{18}F]SF51 preparations showed high radiochemical purity (>99%) verified by radio high-performance liquid chromatography (HPLC). No adverse or clinically detectable pharmacological effects were reported in any of the nine participants following [^{18}F]SF51 administration. Details of the injected activity, molar activity, and injected mass dose are provided in Table 1. Vital signs and electrocardiogram readings did not significantly change during the PET scan.

Arterial input function

Unchanged [^{18}F]SF51 peaked around 2 minutes post-administration. LABs demonstrated a peak SUV level (16 ± 2 , $n = 2$) similar to that of HABs and MABs, but with a more gradual decline (Figure 1(a)). The fraction of [^{18}F]SF51 in arterial plasma, measured over time using HPLC, is depicted in Figure 1(b). The plot shows the proportion of the parent compound remaining at various post-injection time points. Symbols and error bars represent the mean and standard deviation for HABs ($n = 2$), MABs ($n = 3$), and LABs ($n = 2$), respectively. The mean f_p value for LABs ($1.66\% \pm 0.7\%$, $n = 2$) did not significantly differ from that of HABs ($1.43\% \pm 0.09\%$, $n = 2$) and MABs ($1.98\% \pm 0.28\%$, $n = 3$) (one-way ANOVA: $p = 0.29$). The plasma radiochromatogram (Figure 1(c)) indicates the presence of a radiochemical that was more lipophilic than the parent compound. This radiometabolite, which was present in the plasma of all participants, had a peak percent composition of $5.6\% \pm 1.5\%$ ($n = 8$) of the total plasma radioactive composition

Table 1. Demographic characteristics and PET scan parameters for nine healthy volunteers injected with [^{18}F]SF51.

Volunteer demographics and PET scan parameters	Whole-body	Brain		
	MAB (n = 2)	HAB (n = 2)	MAB (n = 3)	LAB (n = 2)
Male: Female (n)	1:1	1:1	2:1	1:1
Age (year)	42 (8)	43 (14)	45 (9)	47 (12)
Body weight (kg)	58 (3)	90 (24)	69 (7)	77 (1)
Injected activity (MBq)	135 (83)	191 (11)	188 (8)	190 (3)
Molar activity (MBq/nmol) ^a	70 (12)	76 (2)	76 (7)	78 (6)
Injected mass dose (nmol/kg)	0.032 (0.016)	0.029 (0.01)	0.033 (0.002)	0.032 (0.002)

MAB: mixed-affinity binder; HAB: high-affinity binder; LAB: low-affinity binder.

^aMolar activity as reported at the time of injection; data are presented as mean values with SD in parentheses.

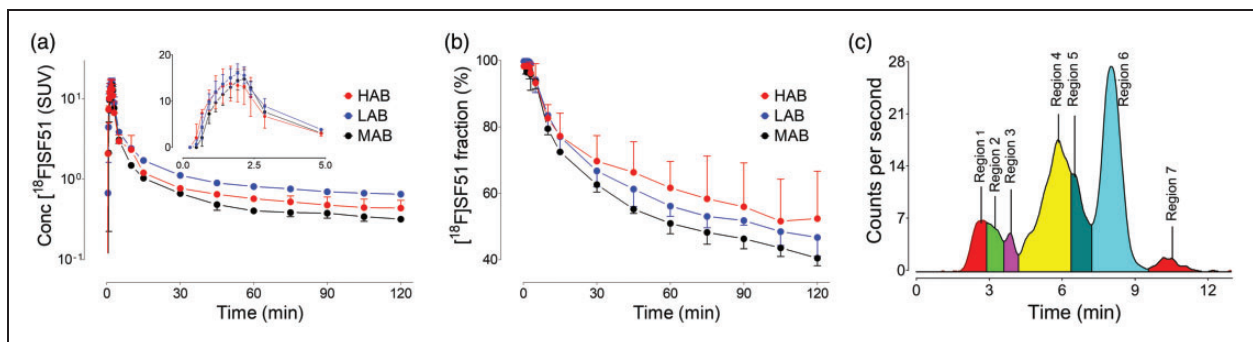


Figure 1. (a) Concentration of [^{18}F]SF51 in arterial plasma was expressed as standardized uptake value (SUV). (b) Fraction of [^{18}F]SF51 in arterial plasma over time, measured using high-performance liquid chromatography (HPLC). This plot demonstrates the proportion of parent compound remaining at different time points post-injection. Symbols and error bars represent mean and standard deviation for high-affinity binders (HABs, $n = 2$), mixed-affinity binders (MABs, $n = 3$), and low-affinity binders (LABs, $n = 2$), respectively. (c) Plasma radio-chromatograms at 120 minutes after injection of [^{18}F]SF51. The presence of a radiometabolite (region 7) more lipophilic than the parent compound (region 6), raises the possibility of radiometabolite brain penetration.

and occurred at $37.5 \text{ min} \pm 16.1 \text{ min}$ ($n=8$) post-radioligand administration.

Brain distribution and kinetics of [^{18}F]SF51

[^{18}F]SF51 demonstrated rapid brain penetration, with peak uptake at 3 to 5 minutes post-injection. All participants showed a similar peak SUV of brain uptake (1.48 ± 0.37), but LABs experienced a quicker wash-out, suggesting lower radioligand retention in the brain (Figure 2). Additionally, a low level of uptake

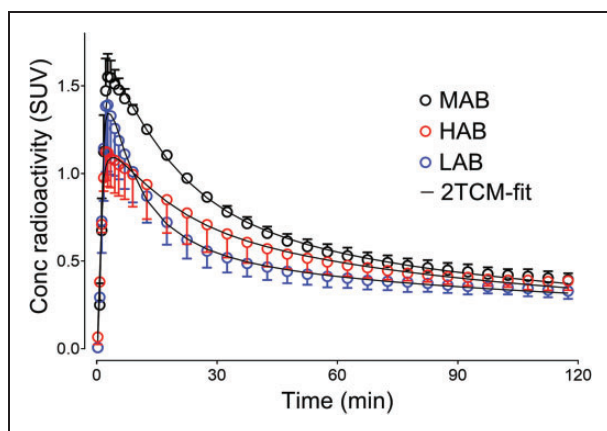


Figure 2. Concentration of radioactivity in whole brain of healthy participants was expressed as standardized uptake value (SUV). Symbols and error bars represent mean and standard deviation (high-affinity binder (HAB): $n=2$; mixed-affinity binder (MAB): $n=3$; and low-affinity binder (LAB): $n=2$), respectively. The brain time-activity curves fitted well by visual inspection using a two-tissue compartment model (2TCM).

was noted in the skull (Figure 3), which was likely attributable to the specific binding to bone marrow rather than deposition of [^{18}F]fluoride into bone from defluorination, as discussed in a previous study.¹⁶

Quantification of [^{18}F]SF51 binding in human brain

[^{18}F]SF51 binding in various brain regions was quantified by measuring V_T using 2TCM. The average V_T in the whole brain was only $0.64 \text{ mL}\cdot\text{cm}^{-3}$ for HABs and $0.94 \text{ mL}\cdot\text{cm}^{-3}$ for MABs and significantly lower for LABs at $0.4 \text{ mL}\cdot\text{cm}^{-3}$ (Supplementary Table S1). The ratios of whole brain between affinity groups were: 0.69 for HAB/MAB, 1.62 for HAB/LAB, and 2.36 for MAB/LAB (Supplementary Table S1).

V_T - Time stability analysis

V_T stability for [^{18}F]SF51 is illustrated in Figure 4. Values normalized to the 120-minute terminal V_T showed stability from 80 minutes post-injection for all affinity groups.

Whole-body biodistribution and radiation dosimetry

Biodistribution and radiation dosimetry from whole-body PET scans of two healthy participants are detailed in Supplementary Figure S1 and Supplementary Table S2. Organ residence times varied, with the urinary bladder recording the highest residence times (0.0410 ± 0.0208 hours) and the gallbladder recording the lowest (0.0020 ± 0.0022 hours). The small intestine and osteogenic cells received the highest radiation doses ($22.8 \pm 3.6 \mu\text{Sv}/\text{MBq}$ and $22.2 \pm 4.5 \mu\text{Sv}/\text{MBq}$, respectively),

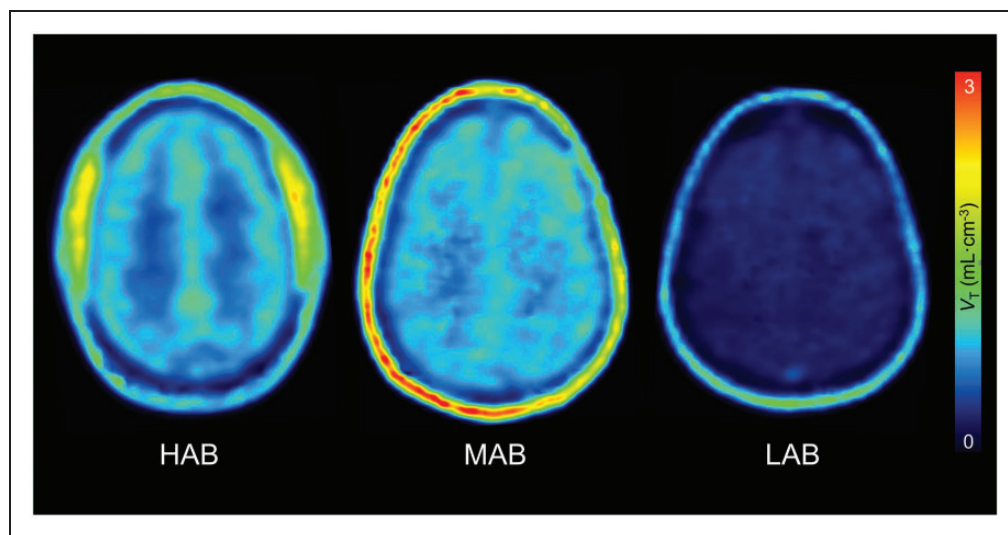


Figure 3. Parametric images of total 18 kDa translocator protein (TSPO) binding (distribution volume (V_T)) for [^{18}F]SF51 in human brain. Each V_T image was generated by Logan Plot using 0–120 minutes of PET data graphical analysis. The Logan plot analysis was conducted with an open parameter fitting approach, allowing t^* to be determined by the model fitting, thus optimizing for the individual kinetic profiles observed.

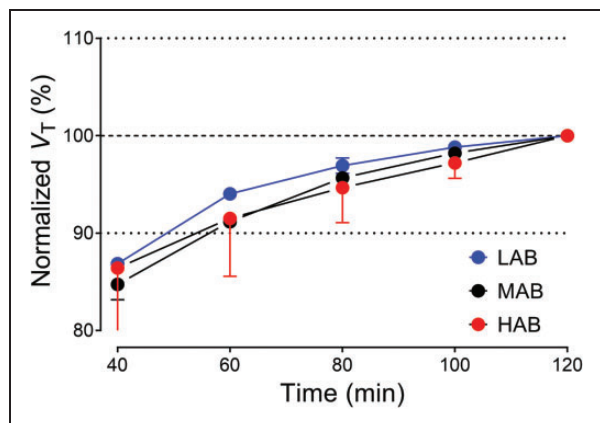


Figure 4. Time-stability analysis of regional total distribution volume (V_T) for $[^{18}\text{F}]\text{SF51}$. V_T was estimated via two-tissue compartment modeling and normalized to the terminal V_T value at 120 minutes. Symbols and error bars represent the mean and SD ($n = 3$ for mixed-affinity binders (MABs); $n = 2$ for high-affinity binders (HABs) and low-affinity binders (LABs)).

while the brain received a lower dose ($5.4 \pm 0.6 \mu\text{Sv}/\text{MBq}$). The effective dose for $[^{18}\text{F}]\text{SF51}$ was calculated at $13.8 \pm 0.9 \mu\text{Sv}/\text{MBq}$ (Supplementary Table S3).

Discussion

This study highlights the limited utility of $[^{18}\text{F}]\text{SF51}$ to quantify TSPO density in human brain, as indicated by the low V_T values across all affinity groups. Specifically, V_T values for HABs and MABs were around $1 \text{ mL} \cdot \text{cm}^{-3}$, significantly lower than those for $[^{11}\text{C}]\text{ER176}^{13}$, reflecting $[^{18}\text{F}]\text{SF51}$'s poor binding capacity. The higher V_T values in MABs compared to HABs might be due to the small number of brain scan participants (two HABs versus three MABs) or yet another paradoxical effect of genotype on radioligand binding to TSPO. The study was stopped after only seven participants had a brain scan because the low uptake in the brain was evident, making further recruitment unnecessary.

The effective dose of $[^{18}\text{F}]\text{SF51}$ was $13.8 \pm 0.9 \mu\text{Sv}/\text{MBq}$, which is in line with the dose delivered by other ^{18}F -labeled radiotracers (average $20.6 \pm 6.8 \mu\text{Sv}/\text{MBq}$).^{20,21} However, comparing $[^{18}\text{F}]\text{SF51}$ with other TSPO tracers such as $[^{11}\text{C}]\text{ER176}$ and $[^{11}\text{C}]\text{DPA-713}$ reveals significant differences in performance. For instance, V_T values for HABs were $3.5 \text{ mL} \cdot \text{cm}^{-3}$ for $[^{11}\text{C}]\text{ER176}^{13}$ and $3.6 \text{ mL} \cdot \text{cm}^{-3}$ for $[^{11}\text{C}]\text{DPA-713}$.²² In contrast, V_T values for $[^{18}\text{F}]\text{SF51}$ were around $1 \text{ mL} \cdot \text{cm}^{-3}$ for both HABs and MABs, indicating substantially lower binding capacity.

The plasma radiochromatographic profile at 120 minutes raises concerns about potential radiometabolites entering the brain (Figure 1(c)). However, V_T

stabilized quickly, which implies both a low level of specific binding for $[^{18}\text{F}]\text{SF51}$ and minimal radiometabolite accumulation in the brain. Regarding the possibility of $[^{18}\text{F}]\text{SF51}$'s radiometabolite accumulation, an *ex vivo* analysis in a mouse was performed, as reported in a previous study,¹⁶ which showed minimal brain radiometabolites and no radio-peak associated with the presence of brain ^{18}F -fluoride. Furthermore, imaging data showing no uptake of radioactivity in skeletal bone of the mouse.

The mouse brain observations and the time-stability in humans support the hypothesis that there was no significant brain radiometabolite accumulation or defluorination. A critical factor in the unexpected failure of $[^{18}\text{F}]\text{SF51}$ in human trials may be attributable to a lipophilic radiometabolite. This radiometabolite, consistently observed at $5.6\% \pm 1.5\%$ in the plasma of all human participants, was notably absent in non-human primate studies. Despite the apparent stability of the time-stability curve, the presence of this radiometabolite could have significant implications for the radioligand's performance in humans. In contrast, all the human arterial plasma samples from both the $[^{11}\text{C}]\text{PBR28}$ and $[^{11}\text{C}]\text{ER176}$ studies lacked the lipophilic radiometabolite that appeared after the parent ligand during reverse-phase separation, as demonstrated by representative radiochromatograms (see Supplementary Figure S2).

The lipophilic nature of this radiometabolite raises concerns about its potential to cross the blood-brain barrier, even in small quantities. If brain penetration occurs, it could lead to two detrimental effects: 1) an increase in nonspecific background signal, potentially masking the true binding of $[^{18}\text{F}]\text{SF51}$ to its target; and 2) a reduction in the overall binding potential of $[^{18}\text{F}]\text{SF51}$, diminishing its efficacy as an imaging agent. These factors, while subtle, could collectively contribute to the observed discrepancy between the promising results observed in animal models and the suboptimal performance in human participants. This finding underscores the importance of comprehensive radiometabolite analysis in translational research and highlights the need for caution when extrapolating results from animal studies to human applications in PET studies.

The low brain uptake in humans observed here was a significant issue for $[^{18}\text{F}]\text{SF51}$ and may be attributable to two main factors. First is the low f_p in humans compared to monkeys. $[^{18}\text{F}]\text{SF51}$ performed better in monkeys ($V_T = 12 \text{ mL} \cdot \text{cm}^{-3}$, $V_T/f_p = 203 \text{ mL} \cdot \text{cm}^{-3}$),¹⁶ a stark between-species difference that could be due to the higher f_p in monkeys ($6.4\% \pm 0.7\%$)¹⁶ versus humans ($1.73\% \pm 0.4\%$). In contrast, f_p values in humans (HABs) were $3.3\% \pm 0.7\%$ for $[^{11}\text{C}]\text{ER176}^{13}$ and $8.0\% \pm 2.2\%$ for $[^{18}\text{F}]\text{DPA-713}$.²² Low f_p means

that a greater proportion of the radioligand is bound to plasma proteins, reducing the amount of free radioligand available to cross the blood-brain barrier. When a significant portion of the radioligand is bound to plasma proteins, it cannot freely diffuse across the blood-brain barrier, leading to lower brain uptake. Examples include [^{11}C]LY2428703, a PET radioligand developed for mGluR1 quantification that, despite promising *in vitro* and *in vivo* results in rodents, was unsuitable for imaging mGluR1s in monkey or human brain due to low brain uptake, likely caused by high binding to plasma proteins.^{23,24} It should be noted that while the f_P of [^{18}F]SF51 was low, it is comparable to that of [^{11}C]PBR28 ($4.8\% \pm 1.7\%$),²⁵ which is recognized as a valid radioligand. Notably, even radioligands with a very low f_P can yield good images if the target receptor is expressed with sufficiently high density.²⁶ Therefore, it is likely that other factors may have contributed to the poor performance of [^{18}F]SF51 in humans.

A second potentially critical factor is binding affinity. The *in vitro* binding affinity (K_i) values were 5.09 nM for [^{18}F]SF51 versus 1.5 nM for [^{11}C]ER176.²⁷ However, the *in vivo* binding affinity (BP_{ND}) values in monkeys were 7.6 for [^{18}F]SF51 versus 8.9 for [^{11}C]ER176. The lower *in vivo* binding affinity for [^{18}F]SF51 compared to [^{11}C]ER176 could be due to the higher nonspecific binding values (V_{ND}/f_P). For [^{18}F]SF51 in monkeys, V_{ND}/f_P was $27 \pm 11 \text{ mL} \cdot \text{cm}^{-3}$ ¹⁶, approximately two-fold that for [^{11}C]ER176 (13.7 to $17.7 \text{ mL} \cdot \text{cm}^{-3}$).²⁷

A third potential factor could be the low penetration of [^{18}F]SF51 across the blood-brain barrier, which might be the case if [^{18}F]SF51 acts as a substrate for efflux transporters, such as P-glycoprotein. Another failed TSPO radioligand, [^{18}F]GE180, showed poor penetration of the blood-brain barrier, presumably for the same reason.^{28,29} Despite these challenges, however, [^{18}F]SF51 yielded much higher V_T values and provided better 2TCM fitting than [^{18}F]GE180.²⁸

Skull uptake was noted in this study, consistent with observations in non-human primate research where skull uptake of [^{18}F]SF51 was inhibited by either of the TSPO ligands (PK11195 and PBR28).¹⁶ This phenomenon was similarly reported in [^{11}C]SF51 monkey imaging studies.²⁷ Furthermore, whole-body imaging in this study revealed pronounced uptake in the pelvis and spine but minimal uptake in other bone tissues, suggesting that the uptake was more likely attributable to specific binding in the bone marrow rather than the deposition of [^{18}F]fluoride ions into bone following defluorination. A recent study found that TSPO expression in the meninges and calvarial bone may

contribute to the skull uptake observed here, even in healthy participants.³⁰ Thus, our findings of [^{18}F]SF51 binding in the skull may reflect intrinsic TSPO expression rather than solely defluorination processes.

Collectively, the data demonstrate that [^{18}F]SF51 is of limited utility for quantifying TSPO density in human brain. The findings also serve to underscore that even when radioligands achieve the necessary parameters on paper, only *in vivo* characterization can provide ultimate proof of the validity of a new radioligand. Nevertheless, animal models are a useful tool when screening for good candidates, even if performance in animals, especially in rodents, may not always predict performance in humans.

Conclusion

Our study highlights significant discrepancies between the preclinical promise and clinical performance of [^{18}F]SF51 as a TSPO-targeted PET imaging agent. Despite promising animal data, [^{18}F]SF51 showed low human TSPO binding and was influenced by the *rs6971* polymorphism. In addition, an unexpected species-specific lipophilic radiometabolite in human plasma, absent in non-human primate studies, likely compromised its performance. These findings emphasize the challenges of developing PET agents and underscore the necessity of: 1) cautious extrapolation from animal models to human outcomes; 2) thorough human *in vivo* characterization, regardless of promising animal results; and 3) detailed radiometabolite analysis across species during development. Collectively, the results from this study underscore the importance of rigorous evaluation in developing reliable PET imaging agents for human use as molecular imaging advances.

Funding

The author(s) disclosed receipt of the following financial support for the research, authorship, and/or publication of this article: This study was funded by the Intramural Research Program of the National Institute of Mental Health, National Institutes of Health [projects ZIAMH002852 and ZIAMH002793].

Acknowledgements

The authors thank the NIH Clinical Center PET Department and the clinical staff of the Molecular Imaging Branch of the NIMH for help in completing the studies, and Ioline D. Henter (NIMH) for invaluable editorial assistance.

Declaration of conflicting interests

The author(s) declared no potential conflicts of interest with respect to the research, authorship, and/or publication of this article.

Authors' contributions

XY: Acquired, analyzed, and interpreted the data; drafted and revised the manuscript; approved the final version of the manuscript.

FS: Acquired and analyzed the data; revised the manuscript; approved the final version of the manuscript.

J-SL: Acquired, analyzed, and interpreted the data; revised the manuscript; approved the final version of the manuscript.

CLM: Acquired and analyzed the data; revised the manuscript; approved the final version of the manuscript.

SJ: Acquired and analyzed the data; revised the manuscript; approved the final version of the manuscript.

JAMS: Acquired and analyzed the data; revised the manuscript; approved the final version of the manuscript.

MJ: Acquired and analyzed the data; revised the manuscript; approved the final version of the manuscript.

SSZ: Acquired, analyzed, and interpreted the data; revised the manuscript; approved the final version of the manuscript.

VWP: Conceptualized and designed the study; acquired, analyzed, and interpreted the data; revised the manuscript for critical intellectual content; approved the final version of the manuscript.

RBI: Conceptualized and designed the study; acquired, analyzed, and interpreted the data; revised the manuscript for critical intellectual content; approved the final version of the manuscript.


PZ-F: Conceptualized and designed the study; acquired, analyzed, and interpreted the data; revised the manuscript for critical intellectual content; approved the final version of the manuscript.

Supplementary material

Supplemental material for this article is available online.

ORCID iDs

Susovan Jana  <https://orcid.org/0000-0001-9910-347X>

Robert B Innis  <https://orcid.org/0000-0003-1238-7209>

References

- Notter T, Coughlin JM, Sawa A, et al. Reconceptualization of translocator protein as a biomarker of neuroinflammation in psychiatry. *Mol Psychiatry* 2018; 23: 36–47.
- Lee JW, Nam H and Yu SW. Systematic analysis of translocator protein 18 kDa (TSPO) ligands on toll-like receptors-mediated pro-inflammatory responses in microglia and astrocytes. *Exp Neurobiol* 2016; 25: 262–268.
- Kim S, Kim N, Park S, et al. Tanycytic TSPO inhibition induces lipophagy to regulate lipid metabolism and improve energy balance. *Autophagy* 2020; 16: 1200–1220.
- Rupprecht R, Wetzel CH, Dorostkar M, et al. Translocator protein (18kDa) TSPO: a new diagnostic or therapeutic target for stress-related disorders? *Mol Psychiatry* 2022; 27: 2918–2926.
- Werry EL, Bright FM, Piguet O, et al. Recent developments in TSPO PET imaging as a biomarker of neuroinflammation in neurodegenerative disorders. *Int J Mol Sci* 2019; 20: 3161.
- Zinnhardt B, Mütter M, Roll W, et al. TSPO imaging-guided characterization of the immunosuppressive myeloid tumor microenvironment in patients with malignant glioma. *Neuro Oncol* 2020; 22: 1030–1043.
- Quach S, Holzgreve A, Kaiser L, et al. TSPO PET signal using [(18)F]GE180 is associated with survival in recurrent gliomas. *Eur J Nucl Med Mol Imaging* 2023; 50: 859–869.
- Nutma E, Gebro E, Marzin MC, et al. Activated microglia do not increase 18 kDa translocator protein (TSPO) expression in the multiple sclerosis brain. *Glia* 2021; 69: 2447–2458.
- Owen DR, Narayan N, Wells L, et al. Pro-inflammatory activation of primary microglia and macrophages increases 18 kDa translocator protein expression in rodents but not humans. *J Cereb Blood Flow Metab* 2017; 37: 2679–2690.
- Nutma E, Fancy N, Weinert M, et al. Translocator protein is a marker of activated microglia in rodent models but not human neurodegenerative diseases. *Nat Commun* 2023; 14: 5247.
- Kreisl WC, Kim MJ, Coughlin JM, et al. PET imaging of neuroinflammation in neurological disorders. *Lancet Neurol* 2020; 19: 940–950.
- Zanotti-Fregonara P, Zhang Y, Jenko KJ, et al. Synthesis and evaluation of translocator 18 kDa protein (TSPO) positron emission tomography (PET) radioligands with low binding sensitivity to human single nucleotide polymorphism rs6971. *ACS Chem Neurosci* 2014; 5: 963–971.
- Ikawa M, Lohith TG, Shrestha S, et al. 11C-ER176, a radioligand for 18-kDa translocator protein, has adequate sensitivity to robustly image all three affinity genotypes in human brain. *J Nucl Med* 2017; 58: 320–325.
- Fujita M, Kobayashi M, Ikawa M, et al. Comparison of four (11)C-labeled PET ligands to quantify translocator protein 18 kDa (TSPO) in human brain: (R)-PK11195, PBR28, DPA-713, and ER176-based on recent publications that measured specific-to-non-displaceable ratios. *EJNMMI Res* 2017; 7: 84.
- Owen DR, Yeo AJ, Gunn RN, et al. An 18-kDa translocator protein (TSPO) polymorphism explains differences in binding affinity of the PET radioligand PBR28. *J Cereb Blood Flow Metab* 2012; 32: 1–5.
- Yan X, Siméon FG, Liow JS, et al. In vivo evaluation of a novel (18)F-labeled PET radioligand for translocator protein 18 kDa (TSPO) in monkey brain. *Eur J Nucl Med Mol Imaging* 2023; 50: 2962–2970.
- Lee JH, Liow JS, Paul S, et al. PET quantification of brain O-GlcNAcase with [(18)F]LSN3316612 in healthy human volunteers. *EJNMMI Res* 2020; 10: 20.
- Zoghbi SS, Shetty HU, Ichise M, et al. PET imaging of the dopamine transporter with 18F-FECNT: a polar

- radiometabolite confounds brain radioligand measurements. *J Nucl Med* 2006; 47: 520–527.
19. Gandelman MS, Baldwin RM, Zoghbi SS, et al. Evaluation of ultrafiltration for the free-fraction determination of single photon emission computed tomography (SPECT) radiotracers: beta-CIT, IBF, and iomazenil. *J Pharm Sci* 1994; 83: 1014–1019.
 20. Zanotti-Fregonara P, Lammertsma AA and Innis RB. Suggested pathway to assess radiation safety of ¹⁸F-labeled PET tracers for first-in-human studies. *Eur J Nucl Med Mol Imaging* 2013; 40: 1781–1783.
 21. Zanotti-Fregonara P, Lammertsma AA and Innis RB. (11)C dosimetry scans should be abandoned. *J Nucl Med* 2021; 62: 158–159.
 22. Kobayashi M, Jiang T, Telu S, et al. (11)C-DPA-713 has much greater specific binding to translocator protein 18 kDa (TSPO) in human brain than (11)C- (R)-PK11195. *J Cereb Blood Flow Metab* 2018; 38: 393–403.
 23. Zanotti-Fregonara P, Barth VN, Liow JS, et al. Evaluation in vitro and in animals of a new 11C-labeled PET radioligand for metabotropic glutamate receptors 1 in brain. *Eur J Nucl Med Mol Imaging* 2013; 40: 245–253.
 24. Zanotti-Fregonara P, Barth VN, Zoghbi SS, et al. 11C-LY2428703, a positron emission tomographic radioligand for the metabotropic glutamate receptor 1, is unsuitable for imaging in monkey and human brains. *EJNMMI Res* 2013; 3: 47.
 25. Kreisl WC, Lyoo CH, McGwier M, et al. In vivo radioligand binding to translocator protein correlates with severity of Alzheimer's disease. *Brain* 2013; 136: 2228–2238.
 26. Terry GE, Hirvonen J, Liow JS, et al. Imaging and quantitation of cannabinoid CB1 receptors in human and monkey brains using (18)F-labeled inverse agonist radioligands. *J Nucl Med* 2010; 51: 112–120.
 27. Lee JH, Siméon FG, Liow JS, et al. In vivo evaluation of 6 analogs of (11)C-ER176 as candidate (18)F-labeled radioligands for 18-kDa translocator protein. *J Nucl Med* 2022; 63: 1252–1258.
 28. Zanotti-Fregonara P, Pascual B, Rizzo G, et al. Head-to-head comparison of (11)C-PBR28 and (18)F-GE180 for quantification of the translocator protein in the human brain. *J Nucl Med* 2018; 59: 1260–1266.
 29. Zanotti-Fregonara P, Pascual B, Rostomily RC, et al. Anatomy of (18)F-GE180, a failed radioligand for the TSPO protein. *Eur J Nucl Med Mol Imaging* 2020; 47: 2233–2236.
 30. Hadjikhani N, Albrecht DS, Mainero C, et al. Extra-axial inflammatory signal in parameninges in migraine with visual aura. *Ann Neurol* 2020; 87: 939–949.